

EVOLVING FLUID CIRCULATION WITHIN THE VARISCAN BEJA-ACEBUCHES OPHIOLITE COMPLEX (SE, PORTUGAL)

António Mateus, Jorge Figueiras, Mário Gonçalves and Paulo Fonseca

Dep. Geologia, Faculdade de Ciências da Universidade de Lisboa, Bloco C2, Piso 5, Campo Grande, 1700 Lisboa, Portugal

Keywords: *Polyphase metasomatism, carbonatization, element mobility, Variscan suture, Upper Paleozoic. Portugal.*

ABSTRACT

The Beja-Acebuches Complex is an extremely dismembered ophiolite sequence incorporated in the Variscan South Iberian Suture, representing a small marginal (back-arc) basin formed during subduction under the Iberian Terrane of normal oceanic crust to the south. Widespread textural evidence for high-temperature (800-900 °C) recrystallization of the basal and intermediate sections of the ophiolite sequence under an anisotropic stress field, suggests that these rocks were obducted before their total consolidation. The later history of this Complex reflects mainly Variscan metamorphism, that peaked at amphibolite facies, and its subsequent waning stages (during which the prevalent hydration of peridotites took place). The final stages of the retrograding path occurred at temperatures below 300 °C and are mainly ascribable to large-scale and repeated H₂O, CO₂ and (subordinate) SiO₂ introduction into the system through WNW-ESE left-handed vertical shear zones, reactivated under brittle conditions with a left-lateral thrusting movement. This large volume, extremely well focused, fluid inflow generally induced very intense carbonatization of the adjoining rocks, with almost total destruction of their original mineralogy and textures and deposition of ankerite + dolomite ± siderite ± magnesite in subsidiary distensive structures. When affecting serpentinized peridotites, this metasomatic process leads to deserpentinization with development of strongly silicified carbonate aggregates. Later hydrothermal events are typically related to the precipitation of microcrystalline quartz and/or calcite in late veins and veinlets. Fluids circulating through the shear zones must have been quite pure, slightly acidic H₂O-CO₂ mixtures, whose very scarcity in metals promoted the hydrolysis of primary minerals and the removal of Al as aqueous-complexes. The origin of these fluids is believed to be related mainly to degassing of the autochthonous carbonate/schist units during Variscan metamorphism and the Beja Igneous Complex intrusion.

INTRODUCTION

Hydrothermal alteration processes involving carbonatization, silicification, and sometimes K-metasomatism, can easily be recognized in many ophiolite sequences, irrespective of their age and of the mechanisms invoked for their emplacement (e.g., Halls and Zhao, 1995, and references therein). However, as far as can be judged from the published data, these geological processes are usually characterized by the introduction of chemical components, and so by rich metasomatic mineral parageneses (e.g., listwaenites). In the Beja-Acebuches Ophiolite Complex (BAOC), late fluid circulation left a relatively complete record in space and time of replacement of primary silicate and oxide minerals by carbonates of variable composition (± secondary silicates). This metasomatic mineralogical record indicates a chemically depleted fluid system whose origins and circulation regimes are the focus of the present work. The main structural control and the mineralogical record of the polyphase metasomatism that affects the ultramafic and mafic rocks of BAOB are examined in order to: 1) evaluate the extent of the metasomatic processes; 2) establish the main physico-chemical constraints imposed on the hydrothermal fluids; and 3) determine the evolution of the hydrothermal system after ophiolite emplacement.

GEOLOGICAL BACKGROUND

The ultramafic-mafic rocks outcropping along the southern border of the Iberian Massif between Ferreira do Alentejo - Beja (Portugal) and Acebuches - Aracena (Spain), represent an extremely dismembered, exotic oceanic terrane that, together with the Pulo do Lobo Accretionary Terrane, define an important southern Variscan suture (e.g., Ribeiro et al., 1990; Quesada et al., 1994; Fonseca, 1995) - Fig. 1. Recent characterization of this exotic terrane and subse-

quent reconstruction of its primary architecture (e.g., Quesada et al., 1994), show that the Beja-Acebuches belt has an ophiolite-like lithostratigraphic column, whose geochemical signature has been interpreted as representing a small marginal (back-arc) basin formed during subduction under the Iberian Terrane of normal oceanic crust to the south.

The complete ophiolite sequence is never observed within the BAOB. Indeed, this strongly fragmented belt of mafic and ultramafic rocks comprises distinct structural domains that are bounded by major shear and fault zones and include different lithological sequences representative of particular portions of the entire oceanic crust (Munhá et al., 1986; 1989; Quesada et al., 1994). The lower sections of the ophiolite sequence, best preserved in the westernmost part of the belt (in Portugal), comprise essentially a succession of peridotites (mainly harzburgitic) and gabbroic rocks (both massive and layered varieties), locally intruded by pods and dykes of plagiogranite. Relics of the upper ophiolitic sections, restricted essentially to the eastern part of the belt (especially in Spain), consist mainly of amphibolites; deep marine sediments and sheeted dyke complexes are almost absent.

Usually, rocks of BAOB are affected by amphibolite facies metamorphism, recorded by plagioclase zoning and crystallization of green Mg-hornblende which forms a pervasive WNW-ESE stretching lineation (e.g., Quesada et al., 1994; Figueiras et al., 1998). This metamorphic event, developed under initial temperatures of 600-620°C and pressures not exceeding 2-3 kbar, is recorded in peridotitic rocks only by relics of talc. However, it did not entirely destroy the evidence of early mineral and textural transformations tentatively ascribed to the emplacement of the ophiolite. Indeed, gabbroic rocks (mostly gabbros and gabbro-norites) display strong mineral and textural evidence for early recrystallization under an anisotropic stress field and high temperatures (800-900°C), with the resulting fabrics indicating N-NNE thrust movement (e.g., Quesada et al., 1994). This early event is not usually texturally visible in the peri-

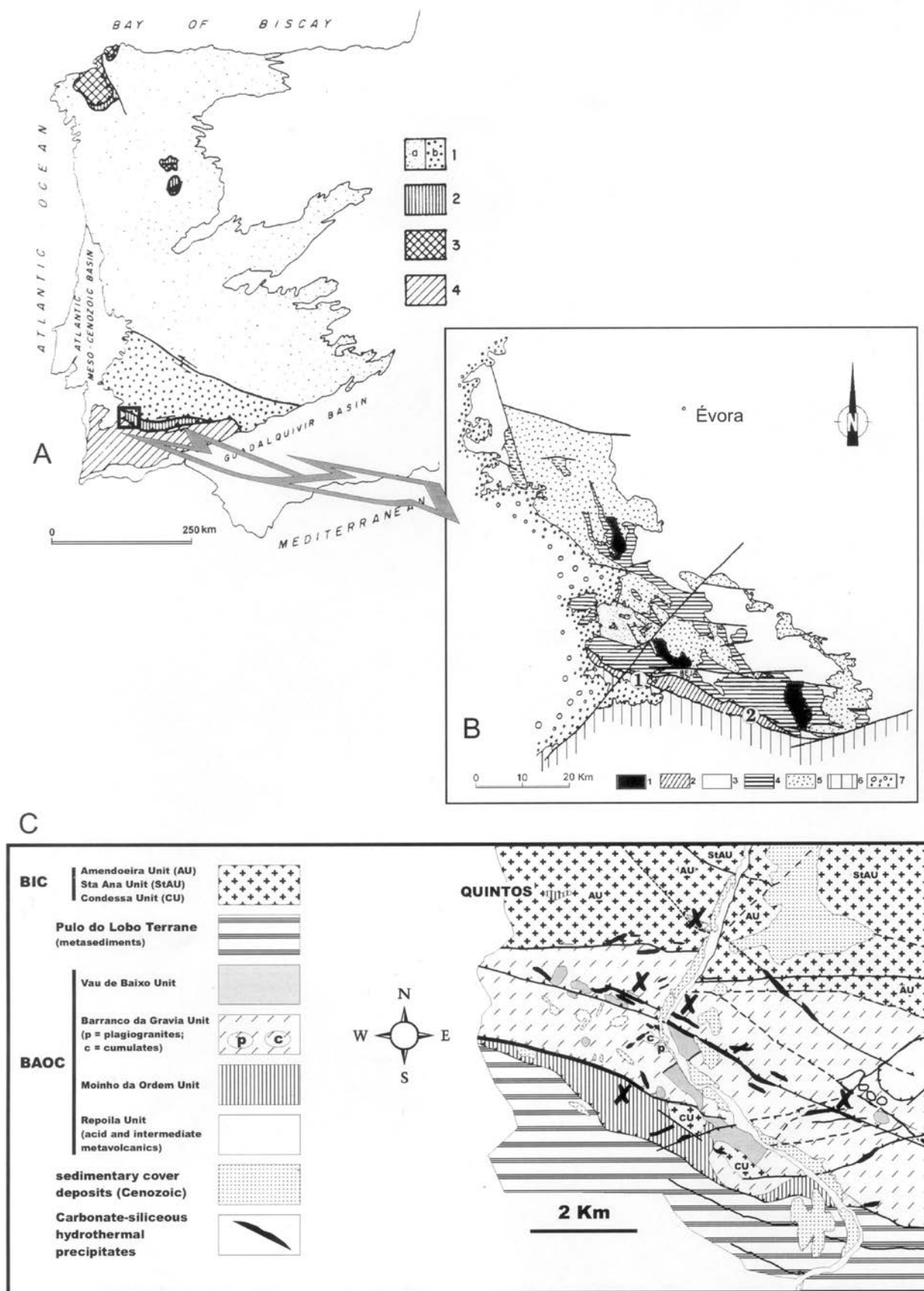


Fig. 1 - A- Simplified tectonostratigraphic terrane map of the Iberian Massif (adapted from Dallmeyer et al., 1993): 1- Paleozoic Iberian Autochthon (a- Proterozoic Iberian Autochthon; b- Late Proterozoic Ossa-Morena Terrane; 2- Paleozoic Oceanic Terranes; 3- Northwest Iberia Continental Exotic Terranes; 4- South Portuguese Terrane. B- Simplified geological map of the Évora-Beja Domain (adapted from Quesada et al., 1994): 1- Undifferentiated Late Proterozoic and Lower Paleozoic metasedimentary rocks; 2- Beja-Acebuches Ophiolite Complex; 3- Undifferentiated units of the Ossa-Morena Zone; 4- Mafic and intermediate plutonic rocks of the Beja Igneous Complex; 5- Acid plutonic and subvolcanic rocks mainly represented by the Baleizão Porphyry, of the Beja Igneous Complex; 6- Pulo do Lobo metasediments; 7- Tertiary detrital cover. Sites 1 and 2 represent the two main studied areas of BAOC. C- Simplified geological map of area 2 (the Gadiana Valley area) with X indicating the five sectors examined in detail.

dotites (because of widespread serpentinization), but Cr-spinels of slightly anomalous composition record chemical modifications at similar temperatures. Therefore, BAOC obduction occurred at very high residual magmatic temperatures and caused extensive anisotropic recrystallization of the lower and intermediate section of the ophiolite sequence, but not of its upper basaltic layers, which lie sufficiently far from the basal movement planes that no significant deviatoric stress was transmitted to them. The heat content of the obducted slab was too small for it to cause significant metamorphism of the underlying autochthonous rocks. The heat would have rapidly dissipated even if conduction was the only cooling mechanism (Gonçalves et al., 1998a).

The strong tectonic fragmentation of the ophiolite can be correlated with the collisional event through which the South Portuguese Terrane was accreted to the Iberian Massif, enabling the development of major transcurrent WNW-ESE shear zones (see, e.g., Quesada et al., 1994, for a comprehensive review). An increasing amount of field and microstructural evidence (e.g., Gonçalves et al., 1997; Mateus et al., 1997) reveals that the main WNW-ESE shear zones now present in BAOC and bounding it to the North and South, were reactivated several times.

In Portugal, the northern boundary of BAOC is commonly obliterated by later intrusives belonging to the Beja Igneous Complex (BIC), emplaced under geodynamic conditions favourable to calc-alkaline magmatic activity which lasted until late Visean times (e.g., Andrade, 1983; Santos et al., 1990; Dallmeyer et al., 1993). Within BIC, several strongly deformed metasedimentary relics of the Iberian Autochthonous Terrane can be recognized. The latter are usually elongate bodies that comprise three main lithostratigraphic sub-units and display an internal imbricated structure, with older rocks on top of progressively younger ones: 1) a dolomitic and/or calcitic marble sequence of Early Paleozoic age (Cambrian?, Andrade et al., 1992); 2) an intermediate sequence mainly composed of amphibole-bearing gneisses (Late Proterozoic?, Fonseca, 1995); and 3) an heterogeneous sequence comprising carbonate rocks, amphibolites and biotite micaschists interbedded with lidites and black quartzites, presumably a lateral equivalent of Série Negra, a well known stratigraphic horizon of Late Proterozoic age very well exposed in a northern belt of the Iberian Autochthonous Terrane. It should be noted, however, that in some of these metasedimentary bodies, several lens-shaped mafic outcrops can be observed within the marble horizons. These rocks, whose whole-rock geochemical signature is similar to that of continental tholeiitic basalts, record a metamorphic path that evolves from eclogitic (≈ 12 kbar, ≈ 550 °C) to transitional epidote-amphibolitic facies (ranging from 6 to 2 kbar, and from 500 to 400 °C); this is believed to represent the evolution of P-T conditions at depth in the continental platform prior to and during BAOC emplacement (e.g., Fonseca et al., 1993; Fonseca, 1995; Araújo, 1995; Pedro, 1996).

SAMPLING, SAMPLE PREPARATION AND ANALYTICAL PROCEDURES

The sampling program was carried out in four representative sectors of the Portuguese segment of BAOC which were previously mapped in detail; samples were taken from characteristic outcrops and, in one sector, from drill-cores of three different boreholes drilled some years ago by the Insti-

tuto Geológico e Mineiro. In order to avoid possible contamination of the samples by mild steel mills, thin rock-slices produced with a diamond saw were wrapped in paper and carefully hammer-crushed to a grain size of 1-2 mm. A tungsten carbide mill was used for finer grinding, thus rendering measured W concentrations meaningless and imparting possible Nb and Y contamination to the samples. Whole-rock analyses were accomplished at the Activation Laboratories Ltd (Canada) as follows: research grade geochemical analyses of 69 elements were performed for non-weathered and variably metasomatized rock samples by running ICP, INAA, ICP/MS and XRF analytical methods; for strongly carbonatized rocks, the "Au+47" analytical package was used, combining INAA and total digestion ICP routines. Table 1 displays some of the most representative results obtained; elements whose concentration is below detection limits were discarded. Estimated errors in precision and accuracy are usually better than 2% and 5-10% for major and trace elements, respectively; errors may increase significantly for concentrations close to the detection limits of the analytical methods employed.

Mineral analyses were performed using a three-channel JEOL-JCXA 733 electron microprobe routinely operated with an accelerating voltage of 15 kV and beam currents of 25 and 15 nA for silicates and carbonates, respectively. Quantitative analyses of sulphides were obtained using a fully automated Cameca CAMEBAX electron microprobe with an accelerating voltage of 15 kV and a beam current of 20 nA. Metallic, natural and synthetic mineral standards were used. In both cases, the quality of the analyses was monitored by analyzing as unknowns those same standards before, during and after each analytical session; the estimated error is less than 2% for all the analysed elements. Tables 2 and 3 report representative data for different mineral species expressed as oxide wt% and cation proportions.

STRUCTURAL CONTROL OF FLUID FLOW

The hydrothermal alteration domains of the ultramafic and mafic rocks of BAOC are usually marked by a brownish to pale-yellow colour corresponding to the development of heterogeneous and polyphase, fine-grained, distinctly silicified, carbonate aggregates. In well exposed sectors, a continuous trend between strongly carbonatized rocks and non-carbonatized protoliths can be seen, the former being mineralogically similar to the common infillings of the major shear zones that bring into contact distinct sections of the ophiolite and/or that constitute the main limits of BAOC.

Recently performed detailed mapping (e.g., Gonçalves et al., 1997) shows that the major shear zones have irregular geometry, sometimes with numerous branches, and comprise different structural corridors developed under distinct deformation regimes. A synopsis of the available data reveals, moreover, that the main regional shear zones (N110-120, dipping to the NNE) are relatively late structures, nucleated in semi-brittle regimes and fully developed in brittle regimes. They have a poorly developed brittle N-S conjugate system, and the local stress fields induced by their propagation led to some subsidiary systems (particularly a N65-70 family). The ductile - semi-ductile earlier shear zones strike N140-145, are conjugated to an N-S, ill-developed, subvertical, ductile system, have poor cartographic expression and can be seen to be locally reworked during the development of the prevailing N110-120 shears. Both

main families of structures are mainly left-lateral shear (fault) zones, but those striking N110-120 have an important thrust component towards the south.

On a regional scale, significant carbonatization is restricted to the immediate vicinity of the N110-120 shear zones and, whenever reliable data exist, it can be seen that serpentinization increases towards these tectonic features. Several common features can be pointed out, irrespective of the type, tectonic style and lateral continuity of the shear zones: (1) the presence of hydrothermal polyphase carbonate aggregates (usually silicified) and/or quartz precipitates within some domains of the shear corridors, wherein relics of dynamically incorporated fragments of the adjoining altered host rocks can also be identified; (2) development of alteration haloes with variable extension and intensity along the tectonic features, leading to significant carbonatization and silicification of the ultramafic-mafic rocks; and (3) establishment of complex, late, brittle deformation patterns, which, in some locations, are clearly ascribable to hydraulic brecciation processes.

PETROGRAPHICAL RECORD OF THE HYDROTHERMAL ALTERATION

Petrographic examination of representative metasomatic rocks reveals that, irrespective of the parent rock, the carbonate matrix comprises isotropic fine- to medium grained dolomite-ankerite aggregates. Various amounts of quartz (commonly corroded and of micrometric size) are always present and, even in completely carbonatized rocks, relics of the most refractory primary minerals (spinel, ilmenite, magnetite) can be found, sometimes along with corroded pre-existing silicate aggregates; late micrometric pyrite, usually partially altered to hematite, is disseminated in some samples. The assemblage dolomite + ankerite \pm magnesite + quartz \pm serpentine \pm Mg-chlorite \pm spinel \pm magnetite \pm pyrite + hematite indicates an ultramafic protolith; textural relationships show also that carbonatization took place after the serpentinization process. A carbonatized gabbro is chiefly composed of ankerite + dolomite + quartz \pm plagioclase \pm Fe(Mg)-chlorite \pm sericite \pm ilmenite \pm magnetite \pm pyrite + hematite + leucoxene.

The mineralogy of the veins that regularly cut the carbonatized rocks typically differs according to different host lithologies. For instance, carbonatized gabbros generally present complex networks of veinlets sealed by ankerite + microcrystalline quartz and siderite + pyrite + microcrystalline quartz aggregates; veinlets with a banded texture are rare (when found, their earlier infillings are sideritic), and those filled with coarse calcite aggregates represent the final stages of hydrothermal fluid circulation in these rocks. Conversely, carbonatized peridotites commonly have veins with banded textures, where the following succession may be totally or partially observed from center to margin: (1) white quartz with large crystals and limpid dolomite aggregates within millimetric vugs; (2) white quartz-dolomite bands or dolomite-magnesite bands; (3) green fine-grained quartz; and (4) dolomite-ankerite aggregates containing relics of serpentine \pm chlorite and randomly distributed late aggregates of pyrite (\pm chalcopyrite) and Fe-chlorite. In some cases, the carbonatized peridotites are cut only by irregular veins sealed by relatively coarse-grained dolomite-ankerite aggregates containing abundant centimetric relics of extremely altered parent rock; these structures are usually cut

by later veinlets of dolomite-magnesite or magnesite.

The mineralogical and textural changes that record the polyphase metasomatism of the ultramafic and mafic rocks can best be determined, however, by examination of slightly to moderately carbonatized rocks.

Usually, peridotites form discontinuous outcrops in tectonic contact with the adjoining gabbros. Relics of primary minerals indicate a predominantly harzburgitic composition, somewhat clinopyroxene-enriched in a few places; former dunites and wehrlites are also present. When present, pyroxene relics are usually rimmed by Mg-hornblende; this mineral may also be interstitial and its presence records the Variscan peak metamorphism, under amphibolite facies conditions. Serpentinization is generally relatively intense and post-dates talc formation in some specimens. It commonly has a characteristic mesh texture, typical of lizardite aggregates. Late serpentinization allowed the development of antigoritic precipitates along irregular veinlets, which also contain micrometric aggregates of Mg-chlorite and scarce carbonates (dolomite-magnesite). In addition to serpentine and relics of primary olivine and enstatite, micrometric grains of more or less altered spinel, pyrrhotite, pyrite, and pentlandite and its alteration products are commonly disseminated in these rocks, irrespective of their degree of serpentinization. Spinel crystals typically are rimmed by subsolidus reequilibration products, composed of ferritchromite and ferritchromite \pm magnetite. Dispersed decimillimetric rods of magnetite, sometimes alongside centimillimetric crystals of awaruite and heazlewoodite (representing products of primary sulphide alteration), are also common within strongly serpentinized rock domains. Progressive replacement of serpentine and of primary silicates by fine-grained dolomite-ankerite aggregates with isotropic fabrics, coupled with and/or followed by sulphide minerals oxidation, records interaction with late CO₂-rich fluids in domains relatively close to the main WNW-ESE shear zones. In moderately carbonatized rocks, significant amounts of micrometric (often corroded) quartz, probably reflecting advanced stages of serpentine breakdown are present. Magnetite and primary spinels are commonly preserved in these rocks. Oxide minerals are typically the only remnant of the parent peridotite, but they are extensively corroded in strongly carbonatized samples. Late silica enrichment, as documented by the presence of millimetric interstitial vugs of microcrystalline quartz and by the development of band textured quartz-dolomite veinlets, can also be observed in moderately to strongly carbonatized peridotites.

Non-carbonatized gabbros consist mainly of variable amounts of plagioclase, diopsidic clinopyroxene, brown Ti- and Na-rich hornblende and, sometimes olivine. Minor and variable amounts of V-rich ilmenite and Ti-rich magnetite, are the main accessory minerals. These are accompanied by subordinate, although ubiquitous, amounts of primary, interstitial, micrometric sulphide grains (mainly pyrrhotite, pyrite and sparse chalcopyrite). The early metasomatic events experienced by these rocks resulted from Variscan metamorphism under amphibolite facies conditions, and are recorded by partial destruction of primary pyroxene and amphibole, by quartz deposition and by late plagioclase zonation. Hence, the green Mg-hornblende and actinolite aggregates formed before the partial saussuritization of plagioclase and the interstitial deposition of Fe(Mg)-chloritic aggregates. Subsequent hydrothermal alteration was apparently restricted to intensely fractured rock domains near the WNW-ESE shear zones, and began by conversion of pyrox-

ene relics and amphiboles to chloritic aggregates; these phyllosilicates often fill arrays of microfractures whose direction and geometric characteristics indicate that they are coeval with the tectonic events responsible for the development of the major carbonatized infillings. Increasing alteration led usually to partial corrosion of plagioclase and to the precipitation of significant amounts of interstitial quartz, ankerite and dolomite. This corresponds to the initial stage of carbonatization which produced extensive isotropic and fine-grained aggregates of ankerite + dolomite \pm siderite in moderately to strongly altered samples. Significant amounts of microcrystalline quartz and relics of different types of phyllosilicates (chlorite \pm sericite) can also be recognized, along with partially preserved grains of magnetite and ilmenite. However, in zones of intense alteration these oxides were partially replaced by hematite + leucoxene aggregates. Pre-existing sulphide grains, were also replaced in this fashion, giving rise to randomly distributed aggregates of hematite, some of which contain relics of pyrite. Gabbros that underwent strong hydrothermal alteration also have a variety of veinlets filled with ankerite + microcrystalline quartz, siderite + pyrite + microcrystalline quartz and by coarse calcite aggregates, formed during the final stages of fluid circulation in the system.

WHOLE-ROCK GEOCHEMISTRY

The bulk-rock geochemistry (Table 1) is complex because of extensive redistribution of many of major, minor and trace elements during alteration. There is, however, a relatively continuous gradation between fresh and hydrothermally altered samples and three main groups of metasomatized rocks can be recognized.

The first group comprises strongly carbonatized rocks which $\text{CaO} > 20$ wt% and $\text{MgO} < 15$ wt%, and that typically have Al_2O_3 abundances below 8 wt%. The second group consists essentially of moderately carbonatized peridotites with variable Al_2O_3 and MgO contents (below 15 wt% and in the range 10-39 wt%, respectively), and relatively low CaO (10-17.5 wt%). The third group comprises mainly carbonatized metagabbros with relatively constant Al_2O_3 (15-18 wt%), MgO (≈ 5 wt%) and CaO (6-11 wt%) contents (Fig. 2a, c). The latter two groups can also be distinguished on the basis of their SiO_2 contents, which are around 45-50 wt% for carbonatized gabbros and between 22.5 and 42.5 wt% for carbonatized peridotites (Fig. 2e); silica was not analysed in the first group of metasomatic rocks, but it should be relatively high due to widespread micrometric (often corroded) quartz in their matrix. All of the hydrothermally altered rocks are strongly depleted in alkalis, with Na_2O always above K_2O , suggesting that both elements are contained in the plagioclase relics.

Not surprisingly, the bulk minor and trace-element geochemistry of metasomatized rocks correlates reasonably well with the inferred protolith composition. A gabbroic protolith is indicated by relatively high Ti and V concentrations, covariant with Fe and, typically, similar to those found in the surrounding non-carbonatized rocks (usually above 3000 and 200 ppm, respectively - Fig. 3a, c). High concentrations of Cr, Ni, Co and, in many cases, Cu (above 1000, 800, 130, 110 ppm, respectively), indicate an ultramafic protolith (Fig. 3b). Ba and Sr distributions are, on the contrary, highly variable, since their concentrations are similar to or somewhat enriched relative to protolith concentra-

tions in slightly to moderately altered samples, but are obviously depleted in strongly carbonatized specimens (Fig. 2b, d). Whenever Y concentrations are high enough not to be significantly affected by mill contamination, it can be seen that Sc and Y distributions are roughly covariant for peridotites, in spite of the differences in Sc/Y for some samples (Fig. 3e). The lack of correlation of these elements with Al_2O_3 (Figs. 3d, f) suggests that Al (or possibly Sc and Y) were mobile during some stages of the hydrothermal alteration of the analysed rocks. Although Al contents prior to carbonatization is difficult to assess (especially for chlorite-rich serpentinites), the mineralogical record supports Al removal from the system in variable amounts.

A comparison of whole-rock analyses of non-carbonatized ultramafic and mafic rocks of BAOC and their metasomatized lateral equivalents, suggests that the common minor and trace elements were not extensively homogenized during metasomatism. Thus, with some exceptions, the minor and trace element geochemistry can be used to infer protolith compositions. However, these data provide no information on the sources of the metasomatizing fluids, because no contributions from the fluids can be discerned.

Interesting additional information is given by the examination of the chondrite-normalized REE patterns if the relative gains or losses of the whole-rock REE are evaluated as a function of: (1) the original REE abundance, their distribution and sites of concentration in the mineral phases within the protolith, and the relative stability of the mineral phases; (2) the REE concentrations in the fluid, the partitioning behaviour of the REE between the mineral phases and the fluid, and the ability of the fluid to transport the REE out of the system; and (3) the ability of metasomatic minerals to accommodate the REE released from the original minerals. The relative importance of these parameters is comprehensively reviewed by Humphris (1986) and Henderson (1986).

Another important factor is the relative immobility of the REE in silicate rock systems, even under metamorphic conditions, in the absence of a suitable fluid phase. This stability allows REE patterns of metamorphic rocks to be used to identify the nature of the protolith. This is particularly important in the present case because we are dealing with rocks that underwent complex metamorphism and metasomatism. There is no reason to believe that significant REE exchanges occurred during Variscan amphibolite facies metamorphism (e.g., Quesada et al., 1994, Figueiras et al., 1998). However, large-scale redistribution of primary REE whole-rock contents may have taken place during carbonatization, due to extensive introduction of CO_2 fluids into the system, leading to REE complexing.

Normalized REE patterns of serpentinitized and fresh dunites and harzburgites are similar to one another, since the REE concentrations in both olivine and orthopyroxene are very low. Thus, the relative and variable REE enrichment obtained for the carbonatized dunites and harzburgites of BAOC is ascribable to the widespread deposition of ankerite-dolomite in equilibrium with REE-bearing carbonic fluids (Fig. 4a-c). The presence of these trace elements (some LREE and Eu, in particular) in metasomatic carbonates, suggests a reducing environment in order to maintain Eu in a divalent state. This interpretation is also compatible with the presence of sulphides (presently represented by poorly preserved pyrite relics).

The metasomatized clinopyroxene-enriched peridotites display two different normalized REE patterns (Fig. 4a). A relative depletion of whole-rock REE characterizes the

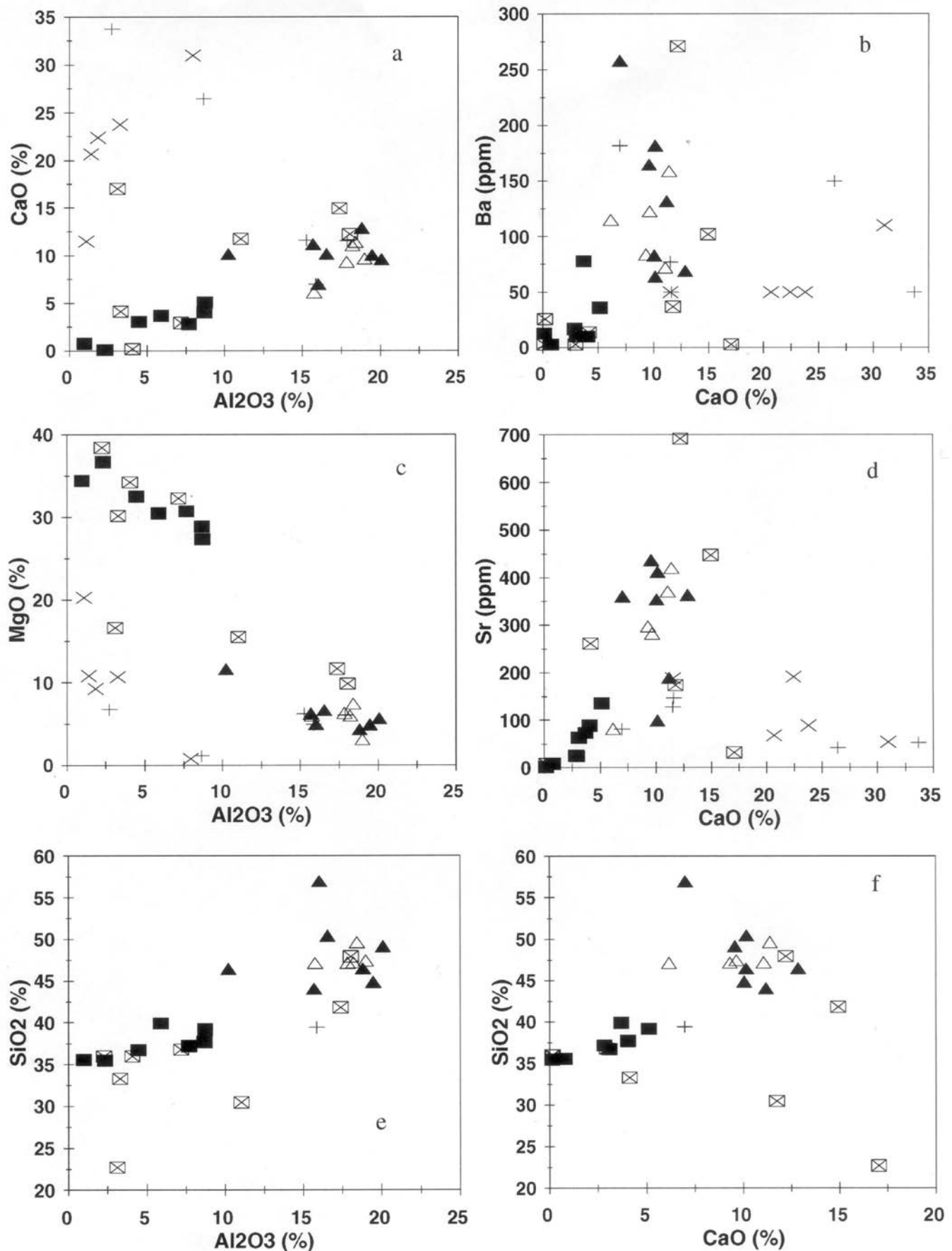


Fig. 2 - Scatter plots for the analysed carbonatized and non-carbonatized rocks of BAOC. Filled squares: non-carbonatized peridotites; Squares with cross: slightly to moderately carbonatized peridotites; Cross signs: strongly carbonatized peridotites; Filled triangles: non-carbonatized gabbroic rocks; Open triangles: slightly to moderately carbonatized gabbroic rocks; Plus signs: strongly carbonatized gabbroic rocks. In samples of Al-rich metasomatized peridotites, chlorite is relatively abundant. Samples of Al-rich metasomatized gabbros contain variable amounts of microrelics of plagioclase, as well as aggregates of hydrothermal chlorite.

Table 1 - Whole rock chemical analysis of representative samples from BAOC

wt%	PERIDOTITE ROCKS					GABBROIC ROCKS												
	NON-CARBONATISED		SLIGHTLY TO MODERATELY CARBONATISED		STRONGLY CARBONATISED		NON-CARBONATISED		SLIGHTLY TO MODERATELY CARBONATISED		STRONGLY CARBONATISED							
	AZM1	FA-13	n=8(*)	AZM5A	FA-24	n=7(*)	TLH-10	STP-10A	n=5(*)	STP15	MAC2	n=7(*)	STP13	S1-14	n=5(*)	MEL-19	MEL-22	n=5(*)
SiO ₂	37.71	35.60	(35.51-39.93)	22.75	41.83	(22.75-47.94)	1.85	1.42	(1.10-7.94)	46.49	49.15	(44.08-56.98)	47.17	49.65	(47.13-49.65)	2.74	8.65	(2.94-17.91)
Al ₂ O ₃	8.68	0.97	(0.97-8.73)	3.10	17.38	(2.27-18.05)	5.58	6.43	(5.29-7.48)	18.82	20.07	(10.24-20.07)	17.85	18.41	(15.75-18.99)	6.35	5.95	(2.04-8.56)
Fe ₂ O ₃	9.21	17.39	(9.21-17.39)	7.72	7.14	(5.41-10.84)	0.24	0.25	(0.08-0.20)	7.36	7.46	(7.10-12.08)	7.38	6.18	(6.18-10.10)	0.47	0.14	(0.05-0.47)
MnO	0.13	0.19	(0.13-0.19)	0.12	0.12	(0.08-0.20)	9.30	10.86	(0.78-20.31)	4.36	5.67	(4.36-11.65)	6.30	7.42	(3.13-7.42)	6.75	1.13	(1.13-6.75)
MgO	28.90	34.43	(27.38-36.71)	16.65	11.67	(9.89-38.43)	0.07	0.05	(0.04-0.08)	12.87	9.58	(7.00-12.87)	9.31	11.40	(6.16-11.40)	33.72	26.43	(6.97-33.72)
CaO	4.04	0.77	(0.12-5.12)	17.04	14.95	(0.12-17.04)	0.02	0.01	(0.01-0.05)	2.84	3.72	(2.40-4.98)	2.51	3.09	(2.51-3.14)	0.31	0.18	(0.07-1.44)
Na ₂ O	0.41	0.04	(0.01-0.81)	0.02	1.23	(0.01-2.43)	0.02	0.01	(0.01-0.05)	0.12	0.47	(0.12-0.62)	0.17	0.28	(0.12-0.98)	0.06	0.02	(0.01-0.40)
K ₂ O	0.01	0.01	(0.01-0.81)	0.03	0.33	(0.01-0.64)	0.02	0.10	(0.02-0.58)	2.29	1.90	(0.83-3.54)	0.85	0.81	(0.81-2.09)	2.42	7.64	(0.10-7.64)
TiO ₂	0.08	0.08	(0.07-0.31)	0.01	0.55	(0.01-0.55)	0.01	0.02	(0.01-0.06)	0.26	0.07	(0.02-0.26)	0.01	0.17	(0.01-0.031)	0.02	0.02	(0.02-0.16)
P ₂ O ₅	0.01	0.01	(0.01-0.07)	0.01	0.08	(0.01-0.08)	0.01	0.02	(0.01-0.06)	3.16	1.92	(1.92-8.34)	8.03	1.86	(1.86-8.62)			
LOI	10.81	10.71	(7.94-13.62)	32.20	4.31	(3.28-32.20)				98.69	100.15		99.69	99.98				
Total	99.99	100.20		99.65	99.59													
%																		
S	0.040	0.155	(0.02-0.16)	0.010	0.010	(0.01-0.08)				0.068	0.010	(0.01-0.07)	0.020	0.014	(0.01-0.11)			
C	0.325	0.094	(0.06-0.33)	7.414	0.189	(0.05-7.41)				0.578	0.239	(0.15-1.51)	1.281	0.064	(0.06-1.28)			
ppm																		
Ba	10	3	(3-78)	3	102	(3-271)	50	50	(50-110)	69	165	(64-258)	84	159	(72-159)	50	150	(50-182)
Sr	89	9	(2-136)	32	448	(3-692)	192	68	(54-192)	364	437	(100-437)	298	420	(82-420)	53	42	(42-147)
Y	1	2	(1-6)	2	20	(1-20)	4	4	(2-24)	7	6	(6-38)	6	17	(6-24)	6	7	(2-29)
Zr	5	6	(5-23)	16	27	(2-27)				9	10	(9-291)	9	56	(9-102)			
V	15	18	(5-58)	19	109	(5-109)	39	29	(20-99)	422	314	(164-595)	185	134	(134-401)	115	95	(48-228)
Cu	33	62	(33-97)	4	7	(4-198)	66	12	(7-66)	38	17	(11-38)	21	40	(21-50)	3	9	(2-22)
Zn	31	78	(31-78)	18	31	(18-76)	117	62	(4-117)	37	36	(36-54)	37	34	(34-55)	9	13	(4-54)
Ni	1286	1217	(759-2181)	1060	187	(187-1884)	1288	1003	(103-1288)	24	21	(13-143)	44	137	(17-137)	18	43	(18-183)
Co	108.0	133.0	(96.7-148.0)	59.7	37.7	(37.7-143.0)	100	63	(26-100)	44.0	43.7	(32.90-70.50)	40.5	48.3	(35.1-48.3)	27	28	(16-28)
Cr	2210.0	1180.0	(1180-3620)	2770.0	437.0	(437-3170)	2300	2700	(840-2700)	74.9	45.0	(40.9-235.0)	158.0	460.0	(44.4-460.0)	18	68	(18-570)
Sc	6.9	9.4	(6.4-13.5)	6.7	35.2	(6-36)	10	5	(4-20)	37.3	36.3	(28.6-67.2)	25.4	30.4	(24.3-38.1)	11	13	(7.4-35.4)
W	54	8	(6-54)	31	72	(5-158)	67	120	(35-120)	109	121	(41-227)	48	198	(33-198)	67	68	(1-68)
La	0.3	0.3	(0.2-2.3)	0.4	6.7	(0.2-6.7)	0.6	1.0	(0.6-5.1)	3.8	2.8	(2.8-30.5)	3.4	9.7	(3.4-14.2)	1.1	1.7	(1.0-8.6)
Ce	1	1	(1-6)	1	20	(1-20)		4	(4-14)	9	7	(7-58)	8	26	(8-38)			
Nd	1	1	(1-3)	1	14	(1-14)				5	4	(4-21)	4	13	(4-17)			
Sm	0.14	0.19	(0.14-0.88)	0.24	3.36	(0.07-3.36)	0.1	0.4	(0.1-2.5)	1.28	0.96	(0.96-5.44)	0.86	3.09	(0.86-4.18)	0.4	0.5	(0.20-4.16)
Eu	0.14	0.08	(0.08-0.70)	0.14	1.35	(0.08-1.35)	0.5	0.3	(0.3-1.1)	0.79	0.96	(0.59-1.58)	0.68	1.06	(0.68-1.15)	0.3	0.6	(0.3-1.4)
Tb	0.2	0.1	(0.2-0.5)	bdl	0.5	< 0.5	bdl	bdl		0.2	0.2	(0.2-1.8)	0.2	0.6	(0.2-0.8)	bdl	bdl	
Yb	0.17	0.23	(0.17-0.70)	0.22	2.13	(0.15-2.13)	0.4	0.4	(0.4-2.8)	0.74	0.72	(0.74-2.48)	0.85	1.9	(0.85-3.43)	0.5	0.5	(0.4-0.5)
Lu	0.03	0.03	(0.03-0.11)	0.04	0.31	(0.02-0.31)	0.06	0.06	(0.06-0.41)	0.11	0.11	(0.11-0.52)	0.13	0.28	(0.13-0.52)	0.08	0.08	(0.06-0.08)

*: total number of analysed samples and respective range of analytical data for each oxide or element; bdl = below detection limit

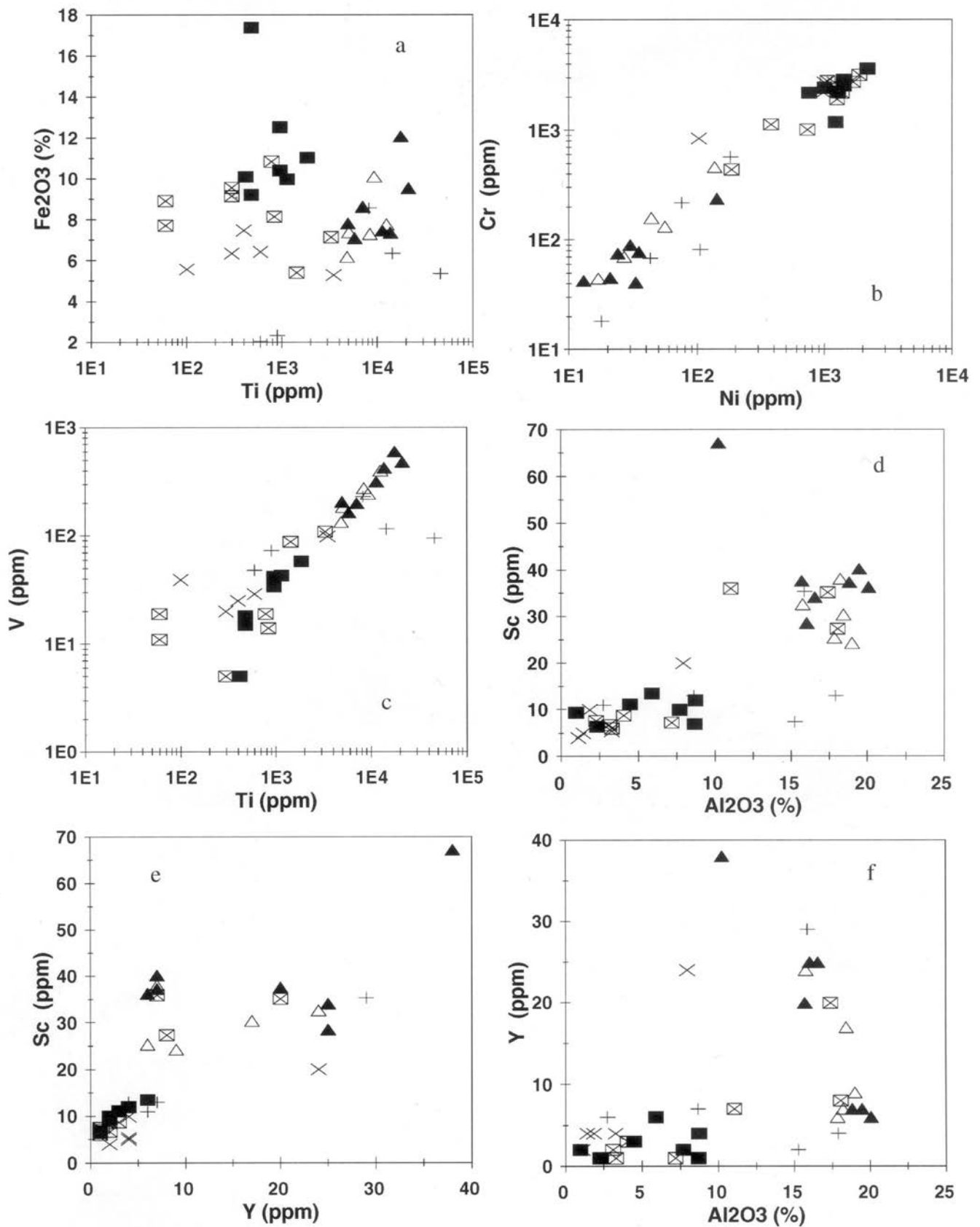


Fig. 3 - Scatter plots for the analysed carbonatized and non-carbonatized rocks of BAOC. Symbols are the same as in Fig. 2.

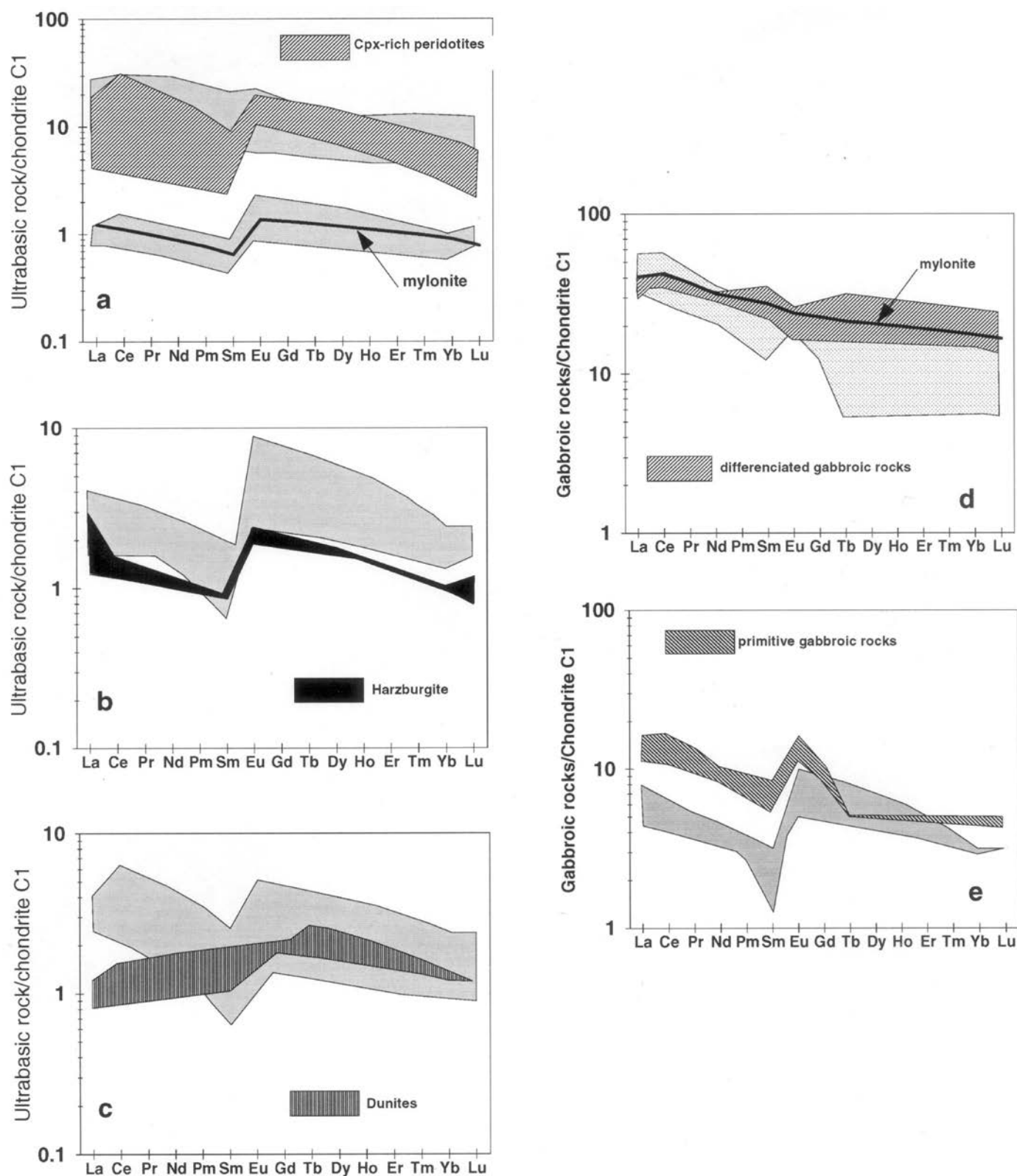


Fig. 4 - Variation ranges of chondrite-normalized REE patterns for peridotite and gabbroic rocks from BAOC. In *d* and *e* the light-grey areas represent the ranges obtained for slightly to moderately carbonatized rocks; the same in *a* for the area that contains the pattern for the sample of mylonite. The remaining light-grey areas of *a*, *b* and *c* correspond to the ranges shown by strongly carbonatized rocks.

slightly to moderately carbonatized samples, including those that exhibit strong deformation (such as the analysed mylonite sample). However, strong carbonatization of the clinopyroxene-enriched harzburgites restores the overall REE contents. Similar conclusions may be drawn from the normalized REE patterns obtained for the differentiated

gabbros, for which a selective mobility of the HREE can be demonstrated for slightly to moderately carbonatized samples (Fig. 4d). There is also a general tendency for REE depletion in metasomatized, but not extensively carbonatized, equivalents of primitive gabbros (Fig. 4e); these normalized REE patterns are compatible with the preservation of signif-

icant amounts of plagioclase.

From the above discussion (in particular from Figs. 4a and 4e) it may be suggested that REE were efficiently mobilized by CO₂-rich fluids during the initial stages of the metasomatism experienced by the ultramafic and mafic rocks of BAOC. Slight relative REE enrichment, or an overall restoration of the primary REE levels, characterizes the strongly carbonatized samples, illustrating the ability of the late carbonate aggregates to accommodate the REE available in the circulating fluid. As is also the case for the remaining minor and trace elements, it is not totally impossible that unchanged but shifted REE patterns simply reflect volume change or shifts in the concentration of another chemical component of the rock during metasomatism. Any quantitative assessment of the chemical exchanges occurring during hydrothermal alteration needs data normalized to some constant factor or evaluated by other means, since in whole-rock analysis no single component is independent of the others. While showing that in the case of BAOC no such reliable constant factor can be found, Gonçalves et al. (1998b) performed several tentative mass balance estimates of the major intervening elements in the carbonatization and silicification processes, according to the method proposed by Gresens (1967).

DISCUSSION

Rocks belonging to BAOC were affected by prominent and polyphase metasomatism whose extent is strongly dependent on the geometry and tectonic activity of the shear zones formed during the late stages of continental collision.

The assemblage dolomite + ankerite ± magnesite + quartz ± serpentine ± chlorite ± spinel ± magnetite ± pyrite + hematite indicates an ultramafic protolith, and shows texturally that carbonatization took place after serpentinization. A gabbroic-derived carbonatized rock is chiefly composed of ankerite + dolomite + quartz ± plagioclase ± chlorite ± sericite ± ilmenite ± magnetite ± pyrite + hematite + leucocoxene. Serpentinization of the peridotites occurred at relatively low temperatures (being coeval with the metamorphic retrograde path recorded in gabbros, *i.e.*, 400–500°C – e.g., Quesada et al., 1994, Figueiras et al., 1998) and produced pseudomorphic-textured lizardite serpentinites in which the minor-element compositions of the primary phases were preserved in the lizardite grains. Olivine was almost completely serpentinized before orthopyroxene was hydrated (Table 2). Concomitant marginal alteration of Cr-spinel, during serpentinization of orthopyroxene, caused release of Cr and Al cations which were incorporated into very fine-grained Mg-chlorite intergrown with serpentine (Table 3).

Carbonatization of BAOC rocks postdates serpentinization and was essentially controlled by the circulation of CO₂-rich fluids along regional WNW-ESE shear zones under temperature conditions roughly below 300 °C. The whole carbonate precipitation sequence seems to reflect a complex interplay between the primary fluid composition and the progressive whole-rock alteration it induced in BAOC rocks. A closer look on this hydrothermal system reveals a rather unusual nature, which needs explanation. The main features are the almost complete lack of minerals other than carbonates (and some quartz) deposited along the shear zones and a gradual evolution of the carbonate compositions from early widespread ankerite/dolomite to late widespread calcite through an intermediate stage, where carbonate com-

position strongly depends on local wall-rock lithology.

Significant fluid circulation began immediately after the peak of regional metamorphism (itself unrelated to ophiolite emplacement) and affected large rock bands near the main shear zones, then evolving in a transitional semi-brittle/brittle regime. The mineralogical record left by these initial fluids is a pervasive serpentinization followed by carbonatization of the host rocks, with decomposition of primary mafic minerals and deposition of carbonates incorporating the metals released. Further evolution of the system led simultaneously to a transition to the brittle regime and to elimination of primary mafic minerals. This resulted in carbonate deposition being restricted to the newly opened veins and veinlets and to a dependence of carbonate composition on the locally available metals, leading to dolomite and/or magnesite precipitation in peridotite-hosted veins and to ankerite/siderite precipitation in gabbro-hosted veins. The final metasomatic stage involved generalized precipitation of calcite together with plagioclase breakdown in gabbros and other basic rocks adjoining the shear zones.

The overall geochemical evidence collected in BAOC metasomatized rocks indicates that carbonatization occurred together with slight silica depletion and strong alumina solution and removal. This very unusual situation poses several geochemical problems.

The general reaction involving silica dissolution is:

$\text{SiO}_2 (\text{s}) + 2 \text{H}_2\text{O} \rightleftharpoons \text{H}_3\text{SiO}_4^- + \text{H}^+$, which is favoured by high *pH* values, given the dissociation of H₄SiO₄ for *pH* values well above 7. Together with the observed carbonate deposition, this might, at first glance, be taken to indicate that alkaline conditions prevailed during metasomatism. However, despite the enhancing effect of the presence of alkali-earth elements in solution (Berger et al., 1994), silica dissolution was not very intense, probable explanations for this being (Dove and Rimstidt, 1994): 1) H₄SiO₄ dissociation buffers *pH* at values not significantly above neutrality, but still compatible with both carbonate precipitation and Al complexing and removal in solution by OH⁻; and 2) the presence of Al³⁺ in solution would further inhibit silica solubility, because of its adverse action on silica dissolution kinetics.

The overall geochemical evidence also shows that, chemically, the fluid must have been dominated by water and CO₂ and remained very low in other chemical components during the whole metasomatic process. In fact, metals for carbonate precipitation seem to have been extracted from the metasomatized rocks at all stages, and even to be locally derived in the intermediate stage between complete ferromagnesian mineral decomposition and the onset of plagioclase hydrolysis. Due to the presence of CO₂ in water, such a fluid would be slightly acidic, not alkaline, and able to partially leach the rocks it percolates through. Accordingly, besides carbonates, whose presence in slightly acidic environments can be expected if the acidity is caused by large amounts of CO₂, some silica was left behind but no alumina remained.

Permanent Al hydroxyl complexing would need an alkalinizing agent whose identity and source are not easy to deduce in the absence of any mineralogical record of its passage. However, OH⁻ is not the only ligand able to form soluble complexes with Al. If conditions are slightly acidic, quite soluble complexes such as Al(H₂O)₆³⁺ and Al(OH)(H₂O)₅²⁺ may form (Cotton and Wilkinson, 1972). Thus, a possible overall scenario for the observed behaviour is: 1) hydrolysis of primary minerals, favoured by CO₂-in-

Table 2 - Representative chemical analyses for different mineral species (expressed as oxide wt%) and cation proportions

	OLIVINES			PYROXENES			AMPHIBOLES			CHLORITES				
	PLM3	FA13	N=18 n=85	PLM2	STP15	N=15 n=45	PLM1	MAC2	AZM13	N=16 n=82	AZN9	PLM4	MEL18B	N=14 n=42
SiO2	39.88	38.96 (38.17-40.56)		54.89	51.99 (51.20-54.84)		41.67	48.30	53.68 (38.17-56.92)		28.12	32.98	27.92 (25.45-33.87)	
TiO2	0.00	0.01 (0.00-0.04)		0.34	0.44 (0.20-0.60)		3.05	1.04	0.18 (0.00-3.46)		0.15	0.03	0.00 (0.00-0.15)	
Al2O3	0.00	0.00 (0-0.02)		1.18	1.99 (1.18-2.38)		11.70	7.04	2.23 (0.28-13.94)		18.47	10.03	21.40 (20.02-24.70)	
Cr2O3				0.25	0.03 (0.00-0.32)		1.79	0.01	0.03 (0.00-1.87)		0.34	0.03	0.00 (0.00-0.34)	
MgO	45.03	40.95 (40.10-46.99)		30.34	13.93 (13.51-31.00)		15.53	14.65	20.19 (0.11-28.75)		15.13	22.30	11.74 (0.01-30.60)	
CaO	0.00	0.03 (0.00-0.04)		1.53	22.30 (0.39-22.92)		10.75	11.21	5.03 (0.07-27.35)		0.07	0.95	0.09 (0.00-0.95)	
MnO	0.18	0.29 (0.10-0.30)		0.20	0.16 (0.16-0.25)		0.08	0.25	0.32 (0.00-0.59)		0.08	0.15	0.01 (0.01-0.79)	
FeO	14.69	18.93 (11.55-19.90)		9.41	8.82 (4.88-10.18)		6.26	12.33	14.07 (0.25-18.27)		24.72	16.93	24.45 (7.99-28.33)	
NiO	0.23	0.15 (0.14-0.33)		0.04	0.00 (0.00-0.04)		0.07	0.00	0.00 (0.01-0.13)		0.02	0.95	0.00 (0.00-0.10)	
Na2O				0.05	0.34 (0.01-0.39)		3.03	0.96	0.22 (0.01-3.10)		0.00	0.44	0.00 (0.00-0.46)	
K2O				0.00	0.00 (0.00-0.01)		0.32	0.19	0.01 (0.00-0.48)		0.00	0.00	0.00 (0.00-0.46)	
Total	100.01	99.32		98.23	100.00		94.25	95.98	95.96		87.10	84.79	85.61	
S														
Si	1.00	1.00		1.96	1.93		6.23	7.12	7.75		2.85	3.35	2.83	
Ti	0.00	0.00		0.01	0.01		0.34	0.12	0.02		0.01	0.00	0.00	
Al	0.00	0.00		0.05	0.09		2.06	1.22	0.38		2.26	1.20	2.56	
Cr				0.01	0.00		0.21	0.00	0.00		0.03	0.00	0.00	
Mg	1.68	1.57		1.62	0.77		3.46	3.22	4.34		2.29	3.37	1.78	
Ca	0.00	0.00		0.06	0.89		1.72	1.77	0.78		0.00	0.10	0.01	
Mn	0.00	0.01		0.01	0.01		0.01	0.03	0.04		0.01	0.01	0.00	
Fe	0.31	0.41		0.28	0.27		0.78	1.52	1.70		2.10	1.44	2.08	
Ni	0.00	0.00		0.00	0.00		0.01	0.00	0.00		0.00	0.19	0.00	
Na				0.00	0.02		0.88	0.28	0.06		0.00	0.06	0.00	
K				0.00	0.00		0.06	0.03	0.00		0.00	0.06	0.00	
Total cations	2.99	2.99		4.00	3.99		15.76	15.31	15.07		9.55	9.72	9.26	

§ Estimations of the basis of: 3 cations, for olivine; 4 cations, for pyroxenes; (15-Na, K) or (13-K, Na, Ca) cations for amphiboles; and 14 oxygens, for chlorites
N = number of examined samples; n = number of analyses

Table 3 - Representative chemical analyses of Cr-spinels, ilmenites and their alteration products (expressed as oxide wt%) and cation proportions

	Cr-SPINELS										ILMENITE						
	STP8B	PLM2	PLM1	FA17	AZM10	FA13	STP10A	N=25 n=150	AZM13	MAC7	MEL16	STP15	STP12	MAC4	N=17 n=77(*)		
SiO ₂	0.15	0.00	0.00	0.08	0.00	0.15	1.75	(0.04-0.06)	0.10	0.15	0.15	0.15	0.25	0.15	(0.00-0.85)		
TiO ₂	0.21	0.13	0.03	0.58	0.40	3.97	1.78	(0.00-3.97)	44.00	44.69	44.58	44.58	91.52	70.75	(39.28-49.28)		
Al ₂ O ₃	33.38	26.41	37.43	27.35	1.41	6.40	3.02	(0.67-44.84)	0.09	0.01	0.02	0.06	0.04	0.03	(0.00-0.46)		
V ₂ O ₃	0.13	0.13	0.06	0.32	0.17	0.78	0.27	(0.04-0.78)	2.43	1.57	2.36	2.36	5.21	3.51	(1.09-2.98)		
Cr ₂ O ₃	30.03	30.26	22.29	31.28	30.45	17.84	34.22	(3.90-36.03)	0.11	0.00	0.02	0.03	0.39	0.10	(0.00-0.19)		
MgO	12.70	6.97	11.26	7.49	0.18	1.58	0.87	(0.01-13.47)	0.05	0.05	0.08	0.31	0.03	0.04	(0.01-1.13)		
CaO	0.00	0.01	0.00	0.00	0.21	0.00	0.08	(0.00-0.89)	0.00	0.00	0.00	0.00	0.59	0.13	(0.00-1.15)		
MnO	0.28	0.38	0.25	0.38	0.36	0.41	0.42	(0.08-0.70)	1.02	0.79	1.22	0.56	0.02	0.08	(0.00-2.67)		
FeO	21.66	32.89	20.07	30.12	41.97	67.06	46.96	(16.92-67.66)	51.12	50.15	47.41	51.31	0.92	19.69	(41.66-52.35)		
NiO	0.15	0.16	0.08	0.13	0.25	0.11	0.52	(0.00-1.36)	0.05	0.00	0.01	0.01	0.00	0.00	(0.00-0.06)		
ZnO	0.22	0.40	0.32	0.35	12.62	0.24	2.71	(0.00-13.03)	0.00	0.00	0.02	0.03	0.00	0.00	(0.00-0.05)		
Total	98.91	97.74	91.79	98.08	88.02	98.54	92.60		98.36	96.67	95.16	99.40	98.97	94.48			
S																	
Si	0.04	0.00	0.00	0.02	0.00	0.04	0.54		0.01	0.01	0.01	0.01	0.01	0.01			
Ti	0.04	0.03	0.01	0.10	0.10	0.87	0.41		1.72	1.77	1.69	1.69	0.01	0.00			
Al	9.32	7.95	11.04	8.15	0.57	2.19	1.10		0.01	0.00	0.00	0.00	0.01	0.00			
V	0.02	0.03	0.01	0.06	0.05	0.18	0.07		0.10	0.07	0.06	0.09	0.00	0.00			
Cr	5.63	6.12	4.41	6.25	8.32	4.10	8.38		0.00	0.00	0.00	0.00	0.00	0.00			
Fe ³⁺	0.98	1.86	0.52	1.42	6.87	8.56	5.97		0.56	0.49	0.37	0.51	0.00	0.00			
Mg	4.49	2.65	4.20	2.82	0.09	0.69	0.40		0.00	0.00	0.01	0.02	0.00	0.00			
Ca	0.00	0.00	0.00	0.00	0.08	0.00	0.03		0.00	0.00	0.00	0.00	0.00	0.00			
Mn	0.06	0.08	0.05	0.08	0.10	0.10	0.11		0.04	0.03	0.05	0.02	0.00	0.00			
Fe ²⁺	3.31	5.17	3.68	4.94	4.50	6.77	5.52		1.61	1.68	1.72	1.65	0.00	0.00			
Ni	0.03	0.03	0.02	0.03	0.07	0.03	0.13		0.00	0.00	0.00	0.00	0.00	0.00			
Zn	0.04	0.08	0.06	0.06	3.22	0.05	0.62		0.00	0.00	0.00	0.00	0.00	0.00			
Total cations	23.96	24.00	24.00	23.93	23.97	23.58	23.28		3.98	4.00	3.99	3.99	3.99	3.99			

§ Estimations of the basis of 32 oxygens, for Cr-spinels, and 4 cations for ilmenites; Fe³⁺ was estimated assuming ideal stoichiometry.
 N = number of examined samples; n = number of analyses; (*) the range of analytical data does not consider the compositions of the alteration products of ilmenite.

duced acidity; 2) Al mobilization and extraction as aqueous complexes; and 3) precipitation of the liberated metals as carbonates, excess silica being left behind as corroded interstitial quartz. Of course, this does not coincide with the general geochemical behaviour of Al under slightly acidic conditions, for in normal geochemical systems, such pH conditions coincide with minimum Al mobility. Our interpretation is that, in the case of BAOC shear zones, aqueous complexes of Al were stabilized relative to insoluble Al-bearing minerals such as phyllosilicates, because the chemical equilibria involving the available cations were extremely shifted to the carbonate side due to overabundance of CO₂.

Late co-precipitation of microcrystalline quartz and calcite also needs an explanation, because silica and carbonates have opposite solubility gradients with temperature (e.g., Fyfe et al., 1978). However, the problem does not exist in a brittle deformation regime, since seismic failure may cause sudden depressurization of the system leading to sudden huge losses of CO₂ and consequent carbonate precipitation.

A final word on the origin of the metasomatizing fluids is warranted. According to the numerical modelling performed by Gonçalves et al. (1998a), it is very unlikely that BAOC hot emplacement could have generated the fluids responsible for the several carbonate (and silica) hydrothermal precipitates along the major WNW-ESE shear zones, because temperatures high enough to promote degassing of the autochthonous carbonate sequence cannot be maintained for the time interval spanning the ophiolite emplacement and shear zones development. Therefore, fluid genesis should mainly be related to later degassing mechanisms of the autochthonous carbonate/schist units accomplished during Variscan metamorphism and BIC intrusion.

Quesada et al. (1994) and Figueiras et al. (1998) have shown that Variscan metamorphism, BIC intrusion and shear zones development within BAOC (and BIC), are all closely related in space and time, thus providing the adequate heat source. Autochthonous carbonate rock units show ample evidence of metamorphic reactions that led to silicate precipitation (forsterite, diopside, flogopite, wollastonite, tremolite/actinolite, epidote and plagioclase), but detailed studies are still lacking. However, the observed metamorphic mineral associations seem to be equivalent to those found in many places around the world and experimentally related to the release of huge amount of water and CO₂ fluids (e.g., Metz and Trommsdorff, 1968; Greenwood, 1975; Fyfe et al., 1978; Ferry and Burt, 1982; Flowers and Helgeson, 1983; Glassley, 1983; and Ferry, 1991).

CONCLUSIONS

At the South Iberian Suture Zone, marked by the Beja-Acebuches Ophiolite Complex (BAOC), Variscan metamorphism peaked at amphibolite facies conditions. Its waning stages were characterized both by the development of important shear zones and the circulation of significant amounts of fluid, causing extensive alteration and metasomatism. At first, influx of aqueous fluids, more or less controlled by incipient shear zones, caused extensive serpentinization of peridotites. Later, stronger development of shear zones together with an important influx of CO₂ led to strong alteration of the wall rocks of the shear zones, with total or partial carbonatization of the primary rocks and strong leaching of chemical elements unable to precipitate as carbonates. Detailed and integrated petrographic and mi-

croanalytical studies show that, after initial serpentinization, the wall rocks were corroded and replaced by ankerite-dolomite masses; later, carbonate deposition became sensitive to wall rock composition, dolomite and/or magnesite precipitating in ultramafic domains and ankerite and/or siderite in gabbroic domains. The last stage of carbonate precipitation was characterized by overall calcite deposition. Comprehensive comparison of carbonate deposition history with the primary mineral decomposition sequence shows that cations for carbonate precipitation were derived from BAOC rocks at all stages of evolution. Also, introduction of chemical elements is not detectable at any stage of this process. On the contrary, mass balance calculations indicate heavy losses of several major elements, particularly aluminium. Thus, the fluids circulating through the shear zones must have been slightly acidic H₂O-CO₂ mixtures quite poor in other chemical components. This scarcity in metals promoted the hydrolysis of primary minerals and the removal of Al as aqueous-complexes. The ultimate origin of the fluids must have been metamorphic degassing occurring during orogenic collision, since numerical modelling shows that the heat input related to BAOC emplacement is grossly inadequate for the amount of autochthonous heating required for such large amounts of fluid generation.

Acknowledgements

The authors gratefully acknowledge Profs. José Munhá and W. S. Fyfe for stimulating discussions on the subject. Many thanks are also due to the Instituto Geológico e Mineiro through the geologists Mr Luís Martins and Mr Victor de Oliveira for providing drill-core sampling, and through Dr Mário Machado Leite for facilities in using the microprobe at the I.G.M. Laboratory. They also express their appreciation to Mr Fernando Santos and to Mr Octávio Chaveiro for the analytical work carried out, respectively, with Cameca CAMEBAX and with JEOL JCXA 733 equipment (the latter at Centro de Geologia - Fac. Ciências Univ. Lisboa). The authors acknowledge the improvements brought in by Dr. Jeff Alt, Dr. Paul Robinson and Dr. Eero Hanski, while peer reviewing the manuscript. The research was supported by a JNICT grant: *MIZOMOR* Project (PBICT/P/CTA/2112/95).

REFERENCES

- Andrade A.A.S., 1983. Contribution à l'analyse de la suture Hercynienne de Beja (Portugal), perspectives métallogéniques. Thèse INPL, Nancy, 137 pp.
- Araújo A., 1995. Estrutura de uma Geotransversal entre Brinches e Mourão (Zona de Ossa-Morena): implicações: implicações na evolução geodinâmica da Margem Sudoeste do Terreno Autóctone Ibérico. PhD Thesis, Univ. Évora, 200 pp.
- Andrade A.S., Antunes M.T., Araújo A., Castro P., Carvalho D., Carvalhosa A., Dias R., Feio M., Fonseca P., Martins L.T., Manuppela G., Marques B., Munhá J.M., Oliveira J.T., Oliveira V., Pais J., Piçarra J.M., Ramalho M., Rocha R., Santos J.F., Silva J.B., Brum A.P. and Zbyszewski G., 1992. Carta Geológica de Portugal na escala 1: 200000, Notícia Explicativa da Folha 8. Serv. Geol. Portugal, 91 pp.
- Berger G., Cadore E., Schott J. and Dove P.M., 1994. Dissolution rate of quartz in lead and sodium electrolyte solutions between 25 and 300°C: effect of the nature of surface complexes and reaction affinity. *Geochim. Cosmochim. Acta*, 58: 541-551.
- Cotton F.A. and Wilkinson G., 1972. *Advanced Inorganic Chemistry*. 3rd ed., Interscience Publishers, New York, 1145 pp.

- Dallmeyer R.D., Fonseca P., Quesada C. and Ribeiro A., 1993. $^{40}\text{Ar}/^{39}\text{Ar}$ mineral age constraints on the tectonothermal evolution of the Variscan Suture in SW Iberia. *Tectonophysics*, 222: 177-194.
- Dove P.M. and Rimstidt J.D., 1994. Silica-water interactions. In: P.J. Heaney, C.T. Prewitt and G.V. Gibbs (Eds.), *Silica - Physical behaviour, geochemistry, and material applications*. Mineral. Soc. America, *Reviews in Mineralogy*, 29: 259-308.
- Ferry J.M., 1991. Dehydration and decarbonation reactions as a record of fluid infiltration. In: D.M. Kerrick (Ed.), *Contact metamorphism*. Mineral. Soc. America, *Reviews in Mineralogy*, 26: 351-393.
- Ferry J.M. and Burt D.M., 1982. Characterization of metamorphic fluid composition through mineral equilibria. In: J.M. Ferry (Ed.), *Characterization of metamorphism through mineral equilibria*. Mineral. Soc. America, *Reviews in Mineralogy*, 10: 207-262.
- Figueiras J., Mateus A., Gonçalves M.A., Fonseca P., 1998. Early deformation and metasomatic evolution of the Barranco da Gravia metagabbros as recorded by amphibole and plagioclase chemistry. *Actas do V Cong. Nacional de Geologia, Comunic. Inst. Geol. Min.* 84 (1): B-91-B-94.
- Flowers G.C. and Helgeson H.C., 1983. Equilibrium and mass transfer during progressive metamorphism of siliceous dolomites. *Am. J. Sci.*, 283: 230-286.
- Fonseca P., 1995. Estudo da Sutura Varisca no SW Ibérico, nas regiões de Serpa-Beja-Torrão e Alvito-Viana do Alentejo. PhD Thesis, Univ. Lisboa, 325 pp.
- Fonseca P., Araújo A., Leal N. and Munhá J., 1993. Variscan Glaucophane-Eclogites in the Ossa-Morena Zone. *Terra Abstracts, Abst. Suppl. 6, Terra Nova*, 5: 11.
- Fyfe W.S., Price N.J., Thompson A.B., 1978. *Fluids in the Earth's Crust*. Elsevier Publ. Co, Amsterdam, 393 pp.
- Glassley W. 1983. Deep crustal carbonates as CO_2 fluid sources: evidence from metasomatic reaction zones. *Contrib. Mineral. Petrol.*, 84: 15-24.
- Gonçalves M.A., Fonseca P., Mateus A. and Figueiras J., 1997. Microstructural characterization of metasomatized gabbroic rocks of the Barranco da Gravia unit (BAOC) at the Guadiana river. 3^a Conf. Annual do Grupo de Geologia Estrutural e Tectónica, Estremoz, Portugal.
- Gonçalves M.A., Mateus A., Figueiras J. and Fonseca P., 1998a. Origin, chemical reactivity and circulation regimes of the CO_2 -(SiO_2) fluids responsible for the polyphasic metasomatism at the Beja-Acebuches Ophiolite Complex. *Actas do V Cong. Nacional de Geologia, Comunic. Inst. Geol. Min.* 84): B-87-B-90.
- Gonçalves M.A., Mateus A., Figueiras J., 1998b. Some problems concerning mass-balance estimates related to hydrothermally altered cumulates in the lower section of the Beja-Acebuches Ophiolite Complex. *Geochemistry of Crustal Fluids: Characterization of Reactive Transport in Natural Systems*, European Research Conferences, Aghia Pelaghia, 22-27 May, Greece.
- Greenwood H.J., 1975. Buffering of pore fluids by metamorphic reactions. *Am. J. Sci.*, 275: 573-593.
- Gresens R.L., 1967. Composition-volume relationships of metasomatism. *Chem. Geol.* 2: 47-65.
- Halls C. and Zhao R., 1995. Listvenite and related rocks: perspectives on terminology with reference to an occurrence at Cregganbaun, Co. Mayo, Republic of Ireland. *Mineral. Deposita*, 30: 303-313.
- Henderson P., 1986. General geochemical properties and abundances of the rare earth elements. In: P. Henderson (Ed.), *Rare Earth Element geochemistry. Developments in Geochemistry 2*, Elsevier, p. 1-32.
- Humphris S.E., 1986. The mobility of the rare earth elements in the crust. In: P. Henderson (Ed.), *Rare Earth Element geochemistry, Developments in Geochemistry 2*, Elsevier, p. 317-342.
- Mateus A., Figueiras J., Gonçalves M.A. and Fonseca P., 1997. Carbonatization of B.A.O.C.'s basic and ultrabasic rocks (Guadiana Valley): structural control and metallogenetic potential. *Comunic.*, 14 Reunião de Geologia do Oeste Peninsular: 145-151.
- Metz P., Trommsdorff V., 1968. On phase equilibria in metamorphosed siliceous dolomites. *Contrib. Mineral. Petrol.*, 18: 305-309.
- Munhá J., Oliveira J.T., Ribeiro A., Oliveira V., Quesada C. and Kerrich R., 1986. Beja-Acebuches Ophiolite, characterization and geodynamic significance. *Maleo*, 2: 31.
- Munhá J., Ribeiro A., Fonseca P., Oliveira J.T., Castro P. and Quesada C., 1989. Accreted terranes in Southern Iberia: Beja-Acebuches ophiolite and related oceanic sequences. 28th Intern. Geol. Cong., Washington, U.S.A.. *Abst. with Programs*, 2: 481-482.
- Pedro J., 1996. Estudo do metamorfismo de alta pressão na área de Safira (Montemor-o-Novo) Zona de Ossa-Morena. MSc Thesis, Univ. Lisboa, 69 pp.
- Quesada C., Fonseca P.E., Munhá J., Oliveira J.T. and Ribeiro A., 1994. The Beja-Acebuches Ophiolite (Southern Iberia Variscan fold belt): Geological characterization and geodynamic significance. *Bol. Geol. Minero*, 105-1: 4-39.
- Ribeiro A., Quesada C., Dallmeyer R.D., 1990. Geodynamic evolution of the Iberian Massif. In: Dallmeyer, R.D., Martinez-Garcia (Eds.), *Pre-Mesozoic Geology of Iberia*. Springer-Verlag, p. 397-410.
- Santos J.F., Andrade A.A.S., Munhá J., 1990. Magmatismo orogénico varisco no limite meridional da Zona de Ossa-Morena. *Comunic. Serv. Geol. Portugal*, 76

Received, November 26, 1998

Accepted, September 10, 1999